High-Efficiency Wireless Power Transfer for Biomedical Implants by Optimal Resonant Load Transformation

Rui-Feng Xue, Kuang-Wei Cheng, *Member, IEEE*, and Minkyu Je, *Member, IEEE*

***Abstract*—Wireless power transfer provides a safe and robust way for powering biomedical implants, where high efficiency is of great importance. A new wireless power transfer technique using optimal resonant load transformation is presented with significantly improved efficiency at the cost of only one additional chip inductor component. The optimal resonant load condition for the maximized power transfer efficiency is explained. The proposed technique is implemented using printed spiral coils with discrete surface mount components at 13.56 MHz power carrier frequency. With an implantable coil having an area of 25 mm $\times$ 10 mm and a thickness of 0.5 mm, the power transfer efficiency of 58% is achieved in the tissue environment at 10-mm distance from the external coil. Compared to previous works, the power efficiency is much higher and the structure is compact with planar integration, easy to tune, and suitable for batch production, as well as biocompatible owing to no incorporation of ferromagnetic core.**

***Index Terms*—Implantable biomedical devices, inductive power transmission, load transformation, resonant coupling, wireless power transfer.**

I. Introduction

IMPLANTABLE biomedical devices play emerging and promising roles in a variety of monitoring, diagnostic, therapeutic and interventional applications [1]. It is one of important challenges to power such chronic biomedical implants reliably. A battery is often not a good option since no available space exists for an implanted battery expected to operate for years or decades *in vivo*. The use of the battery is limited by its total energy storage capacity and number of recharge cycles because the replacement of the battery requires a surgery and imposes additional trauma on patients. The skin-piercing wiring for power delivery is not a preferable solution either due to the restriction of movement and discomfort caused to patients, as well as the risk of infection. Wireless power transfer to implantable biomedical devices obviating the need of implanted batteries or penetrating wires is the safe and preferred implementation.

Inductive coupling is typically used for wireless powering of biomedical implants [2]–[5]. Two coils, located at the external and internal sides of the human body respectively, are coupled mutually at a short distance. The power transfer efficiency of such a system depends on the quality factor (Q) of the coils and the coupling coefficient (k) between the two coils. Unfortunately, the transfer efficiencies are usually poor due to unfavorable conditions in most biomedical applications. For example, in the neural recording application, the implanted coil is mounted subcutaneously with extremely limited headroom between cortex and skull [6]–[8]. High permeability cores typically used in a transformer to confine the magnetic flux are infeasible here considering the strict size constraint and biocompatibility, which leads to the weak mutual coupling. In addition, the achievable self-inductance and Q of the coils are generally low when the coils are implemented by planar structure for low profile [9]. Caused by small Q and k values, this two-coil coupling system usually suffers from poor power transfer efficiency, which drops sharply with distance.

The efficiency becomes more important taking account of the RF exposure of living tissue and electromagnetic compatibility between the powering link and other nearby communication devices. The allowable tissue exposure to RF electromagnetic fields to avoid overheating is a strong concern because a considerable amount of energy may need to be delivered transcutaneously, well above 10 mW in neural recording applications for instance. The resulting tissue temperature rise must be kept below 1–2°C to avoid cellular damage of the brain. Recommendations of safety levels are defined in the IEEE standard C95.1-2005, ICNIRP and FCC guidelines [10]–[12].

Given the extreme size constraint and the significant level of power required by implants, as well as the tissue safety consideration mentioned above, high efficiency is of great importance for the wireless power transfer in biomedical applications. Our focus in this paper is on the efficiency of inductive coupling itself because it is generally the bottleneck of the overall wireless powering link efficiency. Power transfer circuit blocks such as a power amplifier in the transmitter and a rectifier and a regulator in the receiver are beyond the scope of our discussion.

A well-known efficiency-boosting technique is to add the capacitor to form a resonance at the power carrier frequency [13], [14]. However, the efficiency is just marginally improved in

Manuscript received March 07, 2012; revised June 05, 2012; accepted June 26, 2012. Date of publication August 02, 2012; date of current version March 23, 2013. This work is funded by A*STAR (Agency for Science, Technology and Research) SERC (Science and Engineer Research Council), Singapore, under Grant 1021710161. This paper was recommended by Associate Editor S. Sonkusale.

R.-F. Xue and K.-W. Cheng are with the Institute of Microelectronics, A*STAR, Singapore 117685 (e-mail: xuerf@ime.a-star.edu.sg).

M. Je is with the Institute of Microelectronics, A*STAR, Singapore 117685. He is also with the Department of Electrical and Computer Engineering, National University of Singapore, Singapore 117576 (e-mail: jemk@ime.a-star.edu.sg).

Color versions of one or more of the figures in this paper are available online at http://ieeexplore.ieee.org.

Digital Object Identifier 10.1109/TCSI.2012.2209297

practice due to the loading effects which will be discussed later. Recently, research interest in resonance-based energy transfer has been ignited by the MIT's four-coil demonstration featuring high efficiency at midrange as opposed to the conventional two-coil resonant coupling [15]–[18]. The originally presented structure may not be employed directly for biomedical implants due to its bulkiness. A four-coil system specifically for biomedical implants was attempted in [19] with the 2.5-mm thick implanted coil, which may not be acceptable for implanted neural recording applications. A three-coil link is also proposed in [20] with both high efficiency and delivery power. However, the tuning of the coupling between the secondary and load coils is not trivial and the high density AC current induced by the high-Q resonance in the secondary coil may cause damage for the living tissue. Furthermore, litz-wire implementation is not suited for planar integration and batch production.

Silay *et al.* [21] considered the effect of the load resistance on the efficiency. However they derived the optimum load from the conventional resonant coupling structure instead of the general inductive coupling structure and did not decouple the source impedance from the load, and hence they claimed a lower achievable efficiency. Chen *et al.* [22] also studied this problem theoretically and presented a conceptual system. Zargham *et al.* [23] derived a closed-form analytical solution for the optimum load based on the general two-port network theory. In this paper, we present a high-efficiency wireless power delivery technique which can overcome the loading effect and further give the analysis and intuitive physical explanation of the limitation of the conventional resonant coupling. The optimal resonant load transformation is proposed to deliver the required power with maximized efficiency [24], and a concrete implementation suitable for compact planar integration is described in detail. This paper is organized as follows. Section II analyzes the resonant loading condition for maximum power transfer efficiency and discloses the proposed approach. Comparison with the previous work and discussion on tissue effect are also included. Section III describes the design procedure step by step. Experimental verification is presented in Sections IV and V draws the conclusion.

II. Optimal Resonant Load Transformation

A general structure of inductive coupling is illustrated in Fig. 1(a), where L_1 and Q_1 are the self-inductance and the unloaded quality factor of the primary coil respectively, and L_2 and Q_2 are those of the secondary coil. k is the coupling coefficient between the primary and secondary coils. For simplicity, the losses of the capacitors are not included in the figure. A power source drives the primary coil at the carrier frequency ω_c, and the energy coupled by magnetic induction reaches the load Z_L. In practice, a high-efficiency power amplifier is usually used as the source and Z_L consists of the input impedances of a rectifier and a regulator in subsequent stages. Referring to the definition of the operating power gain in [25], here we define the *operating* power transfer efficiency η_{op} as the power delivered to the load over the power input to the inductive coupling coils. Then the total efficiency of an inductive power link η_{Total} can be divided into two parts, that is, the efficiency from the source to the inductive coupling coils

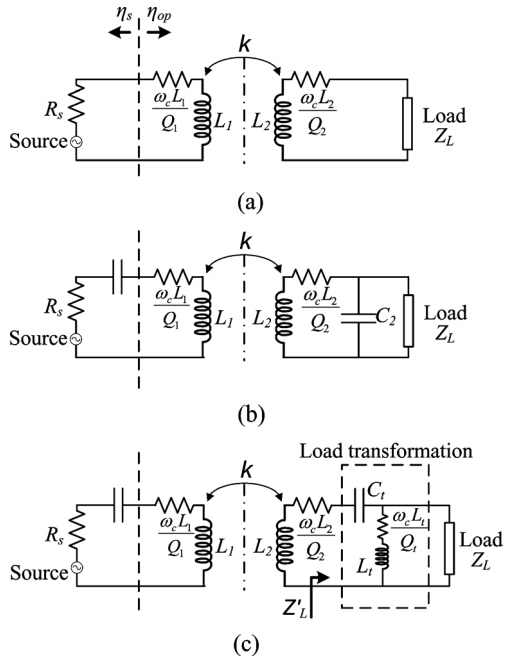

Fig. 1. Schematic of inductive coupling. (a) General inductive coupling. (b) Conventional resonant coupling with loading effect. (c) Proposed resonant coupling with optimal load transformation.

η_s which denotes how efficiently the power amplifier drives the inductive coupling coils [3], [20], [22], [23], [26], and the efficiency from the inductive coupling coils to the load η_{op}.

Based on this general inductive coupling structure, the maximum achievable η_{op} can be derived as

$$\eta_{op\_\max} = \frac{k^2 Q_1 Q_2}{\left(1+\sqrt{1+k^2 Q_1 Q_2}\right)^2} \tag{1}$$

which is a function of unloaded Q and k [13], when Z_L equals to

$$Z_L^{opt} = Z_{Re}^{opt} + jZ_{Im}^{opt} = \frac{\omega_c L_2\sqrt{1+k^2 Q_1 Q_2}}{Q_2} - j\omega_c L_2. \tag{2}$$

Equation (2) is defined as the optimal load to achieve maximum operating power transfer efficiency. This optimal load only depends on the inductive coupling itself and does not relate to the source impedance. Obviously from (1), $\eta_{op\_\max}$ can approach 100% in theory as long as $k^2 Q_1 Q_2 \gg 1$.

Previous works usually focused on increasing Q and k to improve the efficiency according to (1), whereas the condition given by (2) has not drawn enough attention. Actually in most practical applications the efficiencies are limited by the loading effect to a greater extent which will be analyzed in the following. Note that (1) presents the theoretical limit of power transfer efficiency, which can be achieved only when the Z_L has the optimal value given by (2). We will review the conventional resonant coupling from the perspective of (2) and propose the optimal resonant load transformation [24].

A. Conventional Resonant Coupling

A parallel capacitor C_2 is conventionally added to resonate with the secondary coil for efficiency boosting, as shown in

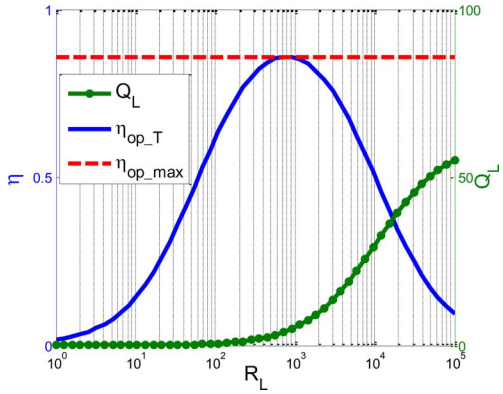

Fig. 2. The power transfer efficiency η_{op_T} and the theoretical limit η_{op_max}, as well as the loaded quality factor Q_L with the load R_L variation (from 1 Ω to 100 kΩ), assuming the resonant frequency $f_0 = 13.56$ MHz, $k = 0.2$, $L_1 = 10$ μH, $Q_1 = 71.0$, $L_2 = 2$ μH and $Q_2 = 60.8$ designed with the procedure in [9] and the EM simulation (HFSS and CST).

Fig. 1(b) [13], [14], [27]–[29]. In the following discussion, R_L will be used instead of Z_L for convenience because the capacitance induced by the load (e.g., rectifier) can be easily absorbed by tuning C_2 during the design process. The power transfer efficiency at resonance is

$$\eta_{op\_T} = \frac{k^2 Q_1 Q_L}{1 + k^2 Q_1 Q_L}\left(1 - \frac{Q_L}{Q_2}\right) \tag{3}$$

where Q_L is the quality factor of the secondary coil loaded by R_L [5]. However, the efficiencies are just marginally improved in most cases. In [17] and [19], this limited efficiency improvement was attributed to the drop of Q_L especially when a heavy load needs to be driven. It is also assumed that a larger R_L will result in a higher Q_L, and thus a higher η_{op_T}.

To investigate this problem, the values of η_{op_T}, η_{op_max} and Q_L are calculated and plotted in Fig. 2 with varying the load. It is found that huge difference exists between η_{op_T} and η_{op_max} except when R_L resides in a specific range. Note that the higher Q_L does not definitely lead to the higher η_{op_T}. For instance, when Q_L is higher than 50 with 100-kΩ load, η_{op_T} is only about 10%, which is pretty low unexpectedly. This can be explained by the fact that η_{op_T} approaches η_{op_max} only when the optimal load condition in (2) is met. C_2 in the conventional resonant coupling structure generates only the imaginary part $-j\omega_c L_2$, without providing any real part to achieve the Z_{Re}^{Opt} of (2). It means that the conventional resonant coupling cannot improve the power coupling efficiency so much when the real part of the load value is not optimal. In order to make η_{op_T} approach η_{op_max}, we need not only to keep the secondary circuit resonant, but also to transform the load to the optimal value given by (2).

As a physical explanation, in a resonant coupling, although it does not change the amount of coupling between L_1 and L_2, the resonance with high Q and low loss can provide high coupling efficiency because the energy that has not been extracted by the load still remains with L_1 and L_2. The source at the primary side only needs to compensate the minor energy loss due to the finite Q of the secondary coil at resonance. In the conventional structure, the secondary parallel tank is equivalent to a current source with high impedance. A smaller R_L is better for energy exaction from the current source, but it degrades the Q of resonance precipitously and deteriorates the efficiency. On the other hand, a larger R_L can keep the high-Q resonance while it cannot exact energy from the tank effectively. This is the reason why the curve of η_{op_T} in Fig. 2 has low values in both low-R_L and high-R_L regions. The proposed optimal resonant loading transformation technique can solve this dilemma properly by mitigating the loading effect to assure the efficient resonance and facilitating the effective power extraction from the tank to the load at the same time.

B. Proposed Optimal Resonant Coupling

Fig. 1(c) shows the schematic of the proposed optimal resonant load transformation. One more inductor L_t is added compared with the conventional structure. L_t and C_t, composing L-transformation, not only resonate with L_2, but also transform the load impedance to the optimal value as in (2), so that η_{op_T} can approach η_{op_max}. Moreover, the proposed scheme is more robust to the load or coupling variations because the gradient of the efficiency curve at this maximum point is zero. Note that the proposed load transformation is different from the conjugate impedance matching which intends to reduce the energy reflection achieving only 50% power transmission efficiency at its maximum.

The desired values of L_t and C_t can be derived by equating the transformed Z_L' in Fig. 1(c) to Z_L^{Opt}

$$L_t = \frac{R_L}{\omega_c \sqrt{\frac{R_L}{\left(\frac{\omega_c L_2}{Q_2}\right)\sqrt{1+k^2 Q_1 Q_2}} - 1}} \tag{4}$$

$$C_t = \frac{1}{\omega_c^2 L_2 \left(1 + \frac{1}{Q_2}\sqrt{\frac{R_L\sqrt{1+k^2 Q_1 Q_2}}{\frac{\omega_c L_2}{Q_2}} - (1 + k^2 Q_1 Q_2)}\right)} \tag{5}$$

Key performance parameters including the operating power transfer efficiency, the voltage transfer ratio defined as the voltage imposed on the load (a rectifier) over the input voltage on the primary coil, and the required source driving capability with respect to the coupling and load variations are analyzed here. The coupling variation may be caused by the coils' displacement or misalignment in vertical and lateral directions. The load is comparatively fixed and will not change dramatically when given a specific application. Typically, the coupling coefficient k ranges from 0.01 to 0.2 and the load resistance R_L has the value between 100 Ω and 100 kΩ depending on applications. For example, a wireless neural recording microsystem consuming about 10-mW average power gives R_L of a few hundreds of ohms, and a wireless implantable blood flow sensing microsystem consuming about 10 μW gives R_L of a few tens of kilo-ohms.

Fig. 3 compares the simulated performances of the conventional parallel and series resonant coupling schemes as well as the proposed one. With the fixed R_L of 200 Ω in Fig. 3(a), the proposed scheme has higher power transfer efficiencies than the other two schemes for varying k, which means the better immunity to displacement or misalignment of the coupling coils.

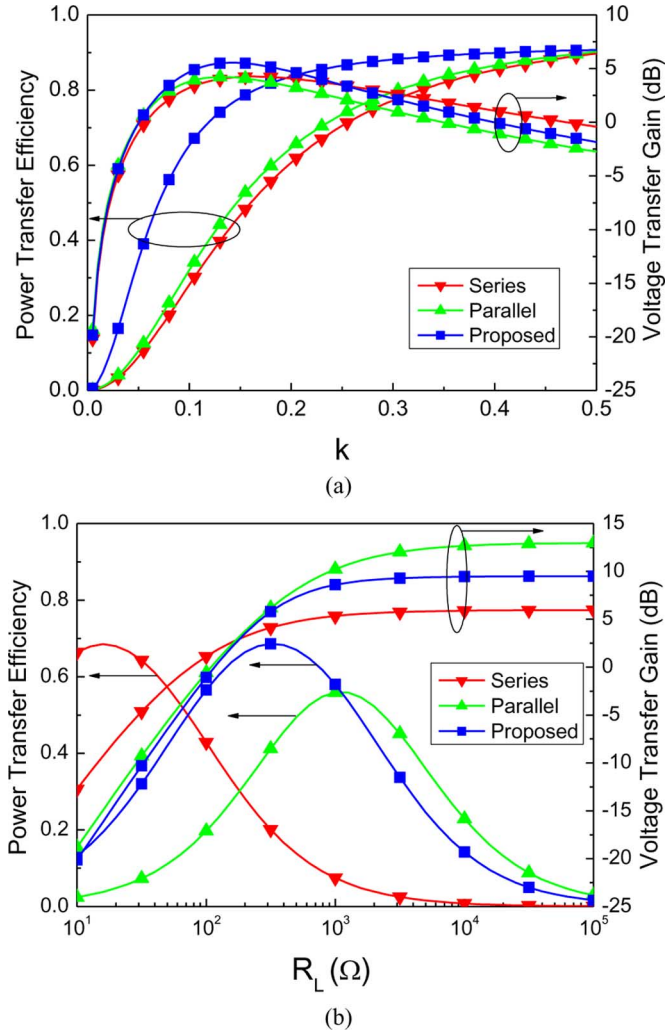

Fig. 3. Simulated performances over (a) coupling k variation (when $R_L = 200\ \Omega$) and (b) load R_L variation (when $k = 0.1$), assuming the parameters of the primary and secondary coils are $L_1 = 18.6\ \mu$H, $Q_1 = 45.2$, and $L_2 = 2.1\ \mu$H, $Q_2 = 68.8$, respectively, designed with the procedure in [9].

Given the fixed k of 0.1 in Fig. 3(b), the efficiencies of the series resonant coupling only with small R_L and the parallel resonant coupling only with large R_L can be high possibly due to insignificant loading effects. In contrast, the efficiency of the proposed scheme can be optimized for any target load values in a given specific application through the tuning of L_t and C_t. Table I summarizes the simulation results of three different wireless power transfer methods illustrated in Fig. 1(a)–(c) for different combinations of k and R_L. It is assumed that the power source impedance $R_s = 50\ \Omega$ (not related to the operating power transfer efficiency) and $\omega_c = 13.56$ MHz. The output power of 10 mW is assumed with ideal power conversion efficiency of subsequent power transfer circuit blocks such as a rectifier and a low-drop-out (LDO) voltage regulator. It is found that the proposed method has higher voltage transfer gain, higher power transfer efficiency, lower source driving requirement, and better immunity to coupling and load variations. The reason behind is that it overcomes the loading effect to maintain efficient resonance and facilitates the effective power delivery from tank to load.

TABLE I
SIMULATION COMPARISON OF THE THREE CASES IN FIG. 1

Performances		$k = 0.2$, $R_L = 50\ \Omega$	$k = 0.05$, $R_L = 200\ \Omega$	$k = 0.05$, $R_L = 500\ \Omega$
Voltage Transfer Gain	(a)	-5.4 dB	-5.7 dB	-3.4 dB
	(b)	-5.2 dB	-2.6 dB	3.8 dB
	(c)	-1.0 dB	2.0 dB	6.2 dB
Power Transfer Efficiency	(a)	30.6%	5.1%	3.3%
	(b)	32.8%	10.9%	22.2%
	(c)	83.5%	38%	48.5%
Source Driving Requirement	(a)	33 mW	196 mW	303 mW
	(b)	30 mW	92 mW	45 mW
	(c)	12 mW	26 mW	21 mW

As (1) and (2) are derived for general inductive coupling configurations, they are also applicable to the four-coil system of MIT [16], [19] or the three-coil system [20], where one more coil is added at the secondary side to realize the optimal resonant loading by adjusting the coupling between the secondary coil and the load coil, and their self-parasitic capacitances. This adjustment is really not trivial. In contrast, we use the transformation network composed of L_t and C_t instead, to implement the optimal loading condition. This approach provides the advantage of much better tunability and compact integration.

III. Compact Planar Implementation

Based on the analysis performed in the previous section, the implementation of wireless power delivery by using the printed spiral coils and chip components is presented in this section. The demonstrated implementation features compact planar integration, excellent tunability and mass manufacturability. The design procedures are outlined with an example of implementation for the neural recording application, where the implant coil locates between the skin and the skull.

A. Identifying Design Constraints

Design constraints of coupling coils are usually specific to a target application and a particular implantable device design. For the target design of the implantable wireless neural recording device in this work, the power required to deliver, the available size and the allowable tissue exposure are summarized in Table II. The printed spiral coil is employed rather than the solenoid coil due to the strict constraint in thickness. It can be precisely defined by lithography on rigid or flexible multilayer substrates, suitable for planar integration and batch fabrication. Ferromagnetic materials used for confining the magnetic flux should be avoided for biocompatibility.

The fact that dielectric property of biological tissue is dispersive and dissipative makes the choice of power carrier frequency and considerations of tissue-induced loss, frequency shift, and tissue safety very important. From the perspective of overall wireless power transfer link efficiency, the power carrier frequency needs to be chosen considering not only the coil coupling, but also the tissue-induced loss and the efficiency of circuit blocks such as the power amplifier and rectifier. The trade-off between the coil coupling and tissue-induced loss is discussed in [30]. The choice of power carrier frequency strongly depends on the allowable coil size, the required power

TABLE II
DESIGN CONSTRAINTS IMPOSED BY APPLICATION

Symbol	Parameter	Design Value
f_r	Operating frequency	13.56 MHz
D_i	Implanted coil dimension (for the neural recording application)	Area = 25×10 mm^2 Thickness = 0.5 mm
d	Transmission distance	10 mm (nominal)
P_o	Received power	10 mW
I_o	Output current	10 mA
SAR	The safety guidelines for specific absorption rate (SAR)	2 W / kg for any 10 g of tissue

level to transfer, and the distance between coupling coils through the tissue medium. In this design, 13.56 MHz is chosen as a carrier frequency.

B. Maximizing k and Q of Coupling Coils

Given the constraints, the design starts with some initial geometry parameters of printed spiral coils and the values are further optimized iteratively to maximize the coupling coefficient k and unloaded Q, as described in [9] in detail. The inductance value of the coupling coils is determined by: (a) the fabrication process and coil size limitations, (b) the desired resonance frequency given by $\omega_0 = 1/(LC)^{0.5}$, and (c) the self-resonance frequency taking the parasitic capacitance into account. In practice, the Q of the coil should be designed considering the trade-off between the efficiency and tolerance.

C. Applying Optimal Resonant Load Transformation

The elements L_t and C_t shown in Fig. 1(c) for optimal resonant load transformation are added on PCB in the form of chip components. Their values are determined by (4) and (5). The effect of living tissue on the transformation component values can be ignored in the design cycle as long as C_t is much larger than the parasitic capacitance induced by the tissue. In addition, the retuning of the inductance value of the coil in previous step may be needed if a proper off-the-shelf component for transformation is not available in practice.

It should be noted that the losses of L_t and C_t are not included in (4) and (5) for simplicity. The limited Q of such components might change their calculated values in practice. Whereas, the influence on the system efficiency is minor since the Q of commercial chip components are usually high enough and the Q of the system need also balance with the tolerance.

Following the procedures mentioned above, the coupling coils are fabricated on PCB with 1-oz copper, as shown in Fig. 4. The Rogers 4350B substrate ($\varepsilon_r = 3.48, \tan\delta = 0.0031$) with a thickness of 0.5 mm is used to reduce the dielectric loss and increase the Q of coils. Given the secondary coil size of 25 mm× 10 mm and 10-mm spacing between the primary and secondary coils in the nominal condition, the primary coil is optimized to the size of 67 mm× 27 mm to make the Q and k as high as possible. The chip components of $L_t = 0.56\ \mu$H and $C_t = 56$ pF for optimal resonant load transformation are soldered on the feeding paths, which are deliberately located at the back side of the coils with offset to avoid direct coupling through them.

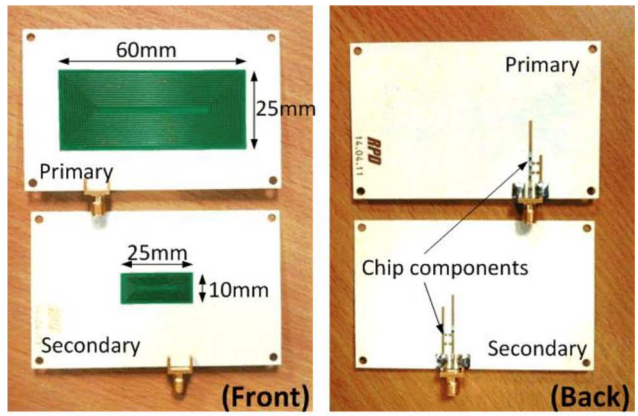

(a)

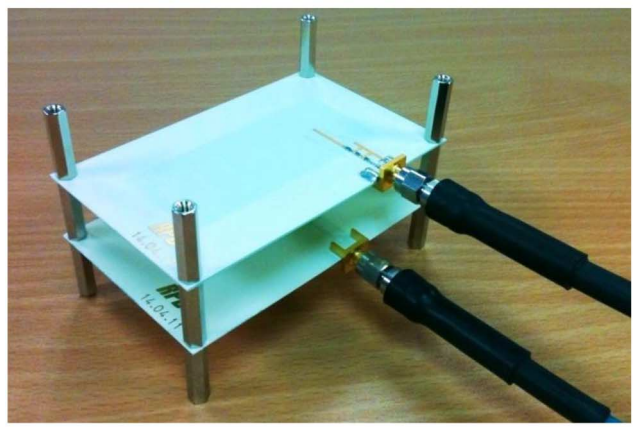

(b)

Fig. 4. The fabricated coils on 0.5-mm thick Rogers 4350B PCB substrate. (a) The primary and the secondary coils: front (left) and back (right). (b) The setup for measurement of coupling through the air.

IV. EXPERIMENTAL RESULTS AND DISCUSSIONS

The fabricated coils can be characterized by measuring its S-parameters. Single-port S-parameter S_{11} is measured using the network analyzer (Agilent E5071B) and converted to the corresponding Z-parameter Z_{11}. Then, the equivalent inductance L, series resistance R and unloaded Q of the coil can be extracted by

$$L = \frac{\mathrm{Im}(Z_{11})}{2\pi f_0} \tag{6}$$

$$R = \mathrm{Re}(Z_{11}) \tag{7}$$

and

$$Q = \frac{\mathrm{Im}(Z_{11})}{\mathrm{Re}(Z_{11})} \tag{8}$$

respectively. The simulated and measured coil properties are summarized in Table III.

A. Measurement of Coupling Performance Through the Air

Both the conventional and proposed structures illustrated in Fig. 1(b) and (c) are fabricated and measured for comparison. An oscilloscope is used to measure input and output voltage

TABLE III
COIL PROPERTIES

Coil Parameters		Simulation	Measurement	Unit
The primary coil	L_1	9.3	9.6	μH
	R_1	7.9	9.9	Ω
	Q_1	100	82	-
	SRF_1	37	31	MHz
The econdary coil	L_2	1.9	2.1	μH
	R_2	3.2	2.6	Ω
	Q_2	51	67	-
	SRF_2	71	65	MHz

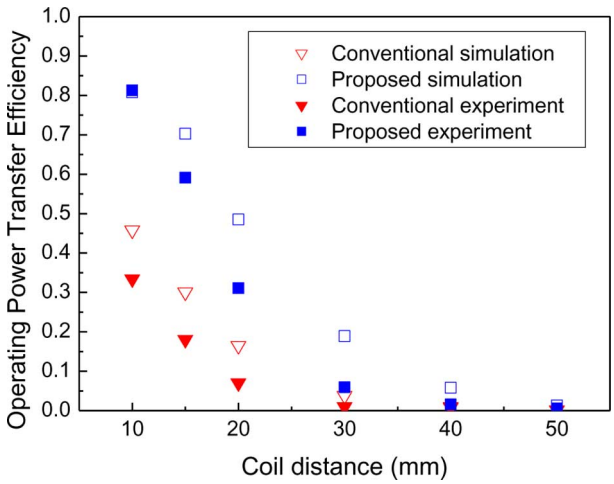

Fig. 5. Power transfer efficiency with different coupling distances in the air environment (the load is an on-chip CMOS rectifier with a typical equivalent $R_L = 200\ \Omega$). Coil fabricated by 1-oz copper on 0.5-mm thick Rogers 4350B substrate. Chip components used for optimal resonant load transformation: $L_t = 0.56\ \mu\text{H}, C_t = 56\ \text{pF}$.

waveforms of the coupling system driven by a signal generator. A small resistance of several ohms is inserted between the source and the coupling system to characterize the input current. Multiplying the input voltage by the input current gives the input power and dividing the squared RMS output voltage by the load produces the output power. The power transfer efficiency is then calculated from the ratio of the output power to the input power. More discussion about the measurement can be referred to [20]. The power transfer efficiency measured with varying the distance between two coils is shown in Fig. 5. The proposed technique exhibits much higher efficiency than the conventional one, achieving the power transfer efficiency of 81% measured with 10-mm distance between the coils. The difference between the simulation and measurement results mainly comes from the Q degradation and the availability of the off-the-shelf matching components in practice. The losses induced by the PCB trace and via, the transition from SMA to PCB trace, the copper loss are not well incorporated in the simulation.

B. Measurement of Coupling Performance Through the Tissue

The effectiveness of the proposed technique in implanted environment is verified here. As shown in Fig. 6, the secondary PCB coil is sandwiched into two pork layers, the sizes of which are much larger than the coil to mimic the practical scenario.

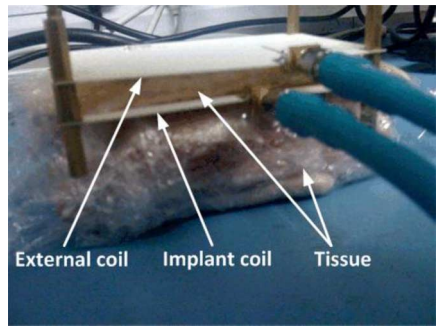

Fig. 6. Measurement setup in the tissue environment.

TABLE IV
MEASURED RESULTS IN TISSUE ENVIRONMENT

Measured at 13.56MHz		Voltage Transfer Gain S_{21} (dB)	Operating Power Transfer Efficiency
10mm spacing	Air	-1.252dB	75.0%
	Tissue	-2.348dB	58.2%
20mm spacing	Air	-6.885dB	20.5%
	Tissue	-7.370dB	18.3%
50mm spacing	Air	-23.578dB	0.44%
	Tissue	-27.921dB	0.16%

For convenience, the two ports of the network analyzer are connected to the primary and secondary coils respectively to measure the transmission coefficient S_{21}. In this case, the voltage transfer gain and the power transfer gain are equal, directly characterized by S_{21}, since the source and load impedances are both 50 ohms. As mentioned earlier, the source resistance may be much larger in this setup than the real application scenario (R_s from 0.1 to 5 Ω for the class-E power amplifier), but the measurement is still effective since the operating power gain and efficiency is independent of the source impedance.

The measured results with different coupling distances in the air and tissue environments are shown in Fig. 7 and summarized in Table IV. The power transfer efficiency of 58% is achieved in the tissue environment at 10-mm distance with the 50-Ω load; while in contrast, the efficiency of the conventional parallel resonant architecture is only 8.7% due to too heavy a loading effect in this case. The loss at 13.56 MHz is estimated to be around 0.1 dB per millimeter of tissue thickness and the frequency shift is roughly 0.3 MHz. The tissue-induced loss and frequency shift are sensitive to the amount of water content in the tissue. For neural recording applications, the implant coil is located below the skin and fat, both of which contain comparatively less water content and cause less effect consequently. This tissue effect can be overcome by intentionally using large component values in the design so that the effect of parasitics caused by the tissue environment can be minimized.

V. CONCLUSION

The limited efficiency of inductive coupling is usually the bottleneck in the efficiency of overall wireless power transfer link from the transmitting source to the final regulated voltage output at the power receiver. Its efficiency is poor especially under unfavorable transcutaneous coupling conditions such as strictly limited space for coil implementation, significant level

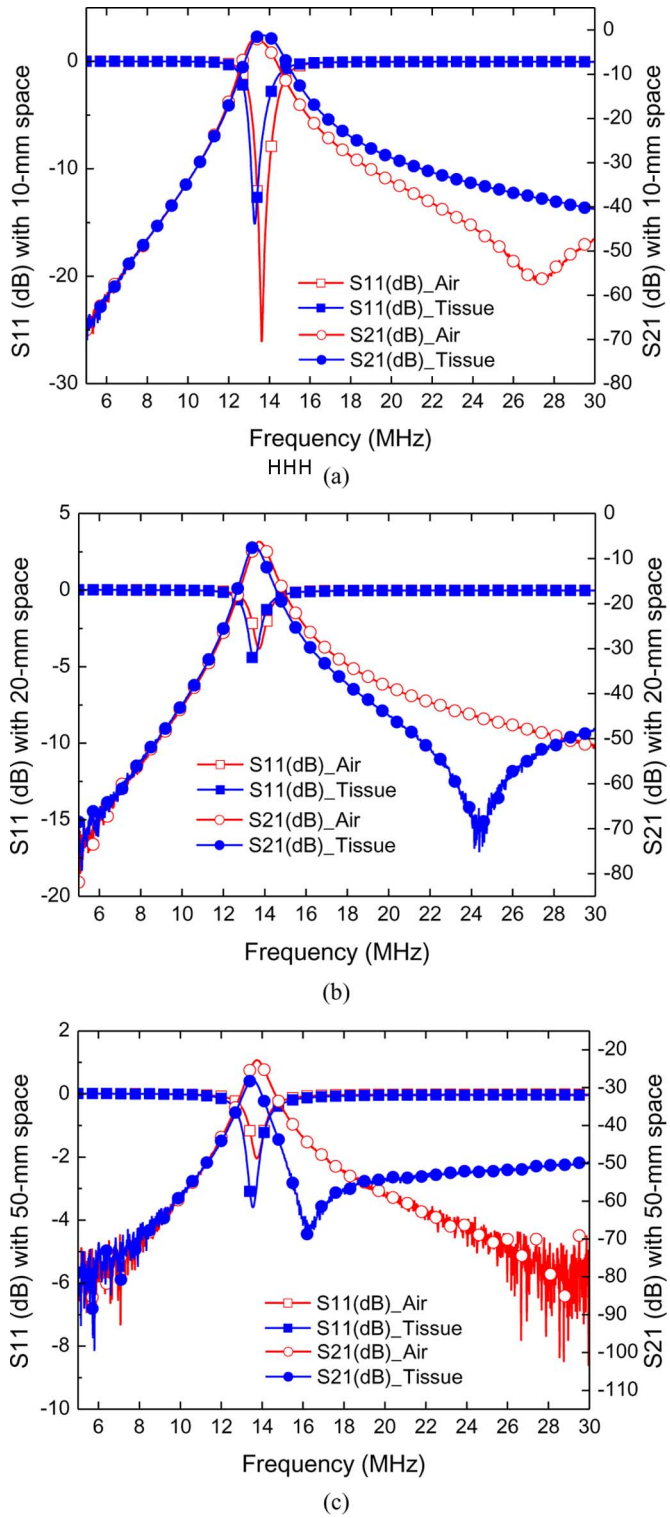

Fig. 7. Measured S_{11} and S_{21} parameters for the coupling through the air and tissue with coupling distances of (a) 10-mm, (b) 20-mm and (c) 50-mm. The operating power transfer gain is equal to S_{21} in this setup.

of power required by implants, as well as tissue safety consideration. A high-efficiency wireless power delivery technique based on optimal resonant load transformation is proposed. Compared with the conventional methods, the proposed technique achieves much higher efficiency and is easy for tuning and integration, robust for coupling and load variations, and biocompatible owing to no ferromagnetic core incorporated.

The technique is developed for, but not confined to biomedical electronics. It can be also used to other applications such as near field communication (NFC) and contactless mobile device charging, where high-efficiency wireless power transfer is needed.

REFERENCES

[1] R. Bashirullah, "Wireless implants," in *IEEE Microw. Mag.s*, Dec. 2010, pp. S14–S23.
[2] K. Van Schuylenbergh and R. Puers, *Inductive Powering: Basic Theory and Application to Biomedical Systems*. New York: Springer Science + Business Media B. V., 2009, ch. 2.
[3] M. W. Baker and R. Sarpeshkar, "Feedback analysis and design of RF power links for low-power bionic systems," *IEEE Trans. Biomed. Circuits Syst.*, vol. 1, no. 1, pp. 28–38, Mar. 2007.
[4] Z. Yang, W. Liu, and E. Basham, "Inductor modeling in wireless links for implantable electronics," *IEEE Trans. Magn.*, vol. 43, no. 10, pp. 3851–3860, Oct. 2007.
[5] R. R. Harrison, "Designing efficient inductive power links for implantable devices," in *Proc. IEEE Int. Symp. Circuits Syst.*, 2007, pp. 2080–2083.
[6] A. M. Sodagar, K. D. Wise, and K. Najafi, "A wireless implantable microsystem for multichannel neural recording," *IEEE Trans. Microw. Theory Tech.*, pp. 2565–2573, Oct. 2009.
[7] R. R. Harrison *et al.*, "A low-power integrated circuit for a wireless 100-electrode neural recording system," *IEEE J. Solid-State Circuits*, vol. 42, no. 1, pp. 123–133, Jan. 2007.
[8] S. B. Lee *et al.*, "An inductively powered scalable 32-channel wireless neural recording system-on-a-chip for neuroscience applications," *IEEE Trans. Biomed. Circuits Syst.*, vol. 4, no. 6, pp. 360–371, Dec. 2010.
[9] U.-M. Jow and M. Ghovanloo, "Design and optimization of printed spiral coils for efficient transcutaneous inductive power transmission," *IEEE Trans. Biomed. Circuits Syst.*, vol. 1, no. 3, pp. 193–202, Sep. 2007.
[10] *IEEE Standard for Safety Levels with Respect to Human Exposure to Radio Frequency Electromagnetic Fields, 3 kHz to 300 GHz*, 2006, IEEE C95.1-2005.
[11] "Guidelines for limiting exposure to time-varying electric, magnetic and electromagnetic fields (up to 300 GHz)," *Health Phys.*, vol. 74, pp. 494–522, 1998.
[12] "Evaluating Compliance With FCC Guidelines for Human Exposure to Radio Frequency Electromagnetic Fields," Federal Communications Commission (FCC), Washington, DC, 1997, Tech. Rep. OET Bull. 65.
[13] W. H. Ko, S. P. Liang, and C. D. F. Fung, "Design of radio-frequency powered coils for implant instruments," *Med. Bio. Eng. Comput.*, vol. 15, pp. 634–640, 1977.
[14] N. D. N. Donaldson and T. A. Perkins, "Analysis of resonant coupled coils in the design of radio frequency transcutaneous links," *Med. Bio. Eng. Comput.*, vol. 21, pp. 612–627, 1983.
[15] A. Karalis, J. Joannopoulos, and M. Soljacic, "Efficient wireless non-radiative midrange energy transfer," *Ann. Phys.*, vol. 323, pp. 34–48, 2008.
[16] A. Kurs, A. Karalis, R. Mofatt, J. D. Joannopoulos, P. Fisher, and M. Soljacic, "Wireless power transfer via strongly coupled magnetic resonances," *Science*, vol. 317, no. 5834, pp. 83–86, Jul. 2007.
[17] B. L. Cannon, J. F. Hoburg, D. D. Stancil, and S. C. Goldstein, "Magnetic resonant coupling as a potential means for wireless power transfer to multiple small receivers," *IEEE Trans. Power Electron.*, vol. 24, no. 7, pp. 1819–1825, Jul. 2009.
[18] A. P. Sample, D. A. Meyer, and J. R. Smith, "Analysis, experimental results, and range adaptation of magnetically coupled resonators for wireless power transfer," *IEEE Trans. Ind. Electron.*, vol. 58, no. 2, pp. 544–554, Feb. 2011.
[19] A. K. RamRakhyani, S. Mirabbasi, and M. Chiao, "Design and optimization of resonance-based efficient wireless power delivery systems for biomedical implants," *IEEE Trans. Biomed. Circuits Syst.*, vol. 5, no. 1, pp. 48–63, Feb. 2011.
[20] M. Kiani, U.-M. Jow, and M. Ghovanloo, "Design and optimization of a 3-coil inductive link for efficient wireless power transmission," *IEEE Trans. Biomed. Circuits Syst.*, vol. 5, no. 6, pp. 579–591, Dec. 2011.

[21] K. M. Silay, D. Dondi, L. Larcher, M. Declercq, L. Benini, Y. Leblebici, and C. Dehollain, "Load optimization of an inductive power link for remote powering of biomedical implants," in *Proc. IEEE Int. Symp. Circuits Systems*, May 2005, pp. 533–536.
[22] C.-J. Chen, T.-H. Chu, C.-L. Lin, and Z.-C. Jou, "A study of loosely coupled coils for wireless power transfer," *IEEE Trans Circuits Syst. II, Exp. Briefs*, vol. 57, no. 7, pp. 536–540, Jul. 2010.
[23] M. Zargham and P. G. Gulak, "Maximum achievable efficiency in near-field coupled power-transfer systems," *IEEE Trans. Biomed. Circuits Syst.* vol. 6, no. 3, pp. 228–245, Jun. 2012.
[24] R.-F. Xue, J. H. Cheong, H.-K. Cha, and M. Je, "High-Efficiency Wireless Powering Link With Large Dynamic Range," Provisional Patent Filed No. 201106464-9, Sep. 08, 2011.
[25] G. Gonzalez, *Microwave Transistor Amplifiers Analysis and Design*, 2 ed. Englewod Cliffs, NJ: Prentice Hall, 1997, pp. 213–213.
[26] P. R. Troyk and M. A. K. Schwan, "Closed-loop class E transcutaneous power and data link for microimplants," *IEEE Trans. Biomed. Eng.*, vol. 39, no. 6, pp. 589–599, Jun. 1992.
[27] C.-S. Wang, G. A. Covic, and O. H. Stielau, "Power transfer capability and bifurcation phenomena of loosely coupled inductive power transfer systems," *IEEE Trans. Ind. Electron.*, vol. 51, no. 1, pp. 148–157, Feb. 2004.
[28] Z. N. Low, R. A. Chinga, R. Tseng, and J. Lin, "Design and test of a high-power high-efficiency loosely coupled planar wireless power transfer system," *IEEE Trans. Ind. Electron.*, vol. 56, no. 5, pp. 1801–1812, May 2009.
[29] R. Jegadeesan and Y. X. Guo, "A study on the inductive power links for implantable biomedical devices," in *IEEE Symp. Antennas Propagat.*, 2010, pp. 1–4.
[30] A. S. Y. Poon, S. O'Driscoll, and T. H. Meng, "Optimal frequency for wireless power transmission into dispersive tissue," *IEEE Trans. Antennas Propagat.*, vol. 58, no. 5, pp. 1739–1750, May 2010.

Rui-Feng Xue received the B.Sc. degree (with distinction) in communication engineering from Taiyuan University of Technology, Taiyuan, in 1999, the M.Sc. degree from Shanghai University, Shanghai, in 2002, and the Ph.D. degree from Shanghai Jiao Tong University, Shanghai, China, in 2005, both in electronics engineering.

From 2005 to 2010, he was a Senior Engineer/Manager with Samsung Electronics Co. Ltd., Suwon, Korea, where he was engaged in the research and development of CMOS RF/analog integrated circuits (ICs). Since 2010 he has been a Scientist with Institute of Microelectronics, Agency for Science, Technology, and Research (A*STAR), Singapore, where he currently acts as a Principle Investigator of the wireless power transfer for implantable biomedical systems. His research interests include CMOS RF/Analog IC, RF and antenna system, and biomedical electronics.

Dr. Xue was awarded the gold prize at the inaugural Chip Design Competition, Singapore, held in conjunction with the 13th International Symposium of Integrated Circuits (ISIC), 2011.

Kuang-Wei Cheng (S'07–M'10) received the B.S. and M.S. degrees from the National Taiwan University, Taiwan, in 2000 and 2002, respectively, and the Ph.D. degree from the University of Washington, Seattle, in 2009, all in electrical engineering.

From 2002 to 2004, he was with MediaTek Inc., Hsinchu, Taiwan. In 2006, he has held internship position in National Semiconductor, Santa Clara, CA. In 2010, he joined Institute of Microelectronics, A*STAR, Singapore, where he is currently a Principal Investigator of Biomedical IC Group in Integrated Circuits & Systems Laboratory. His interests include analog and RF IC design for low power wireless communications and biomedical systems.

Dr. Cheng was a recipient of the Best Student Paper Award of IEEE Radio Frequency Integrated Circuits (RFIC) symposium in 2009 and Analog Devices Outstanding Student Designer Award in 2008.

Minkyu Je (S'97–M'03) received the M.S. and Ph.D. degrees, both in electrical engineering and computer science, from Korea Advanced Institute of Science and Technology (KAIST), Daejeon, Korea, in 1998 and 2003, respectively.

In 2003, he joined Samsung Electronics, Giheung, Korea, as a Senior Engineer and worked on multi-mode multi-band RF transceiver SoCs for GSM/GPRS/EDGE/WCDMA standards. Since 2006 he has been with Institute of Microelectronics (IME), Agency for Science, Technology and Research (A*STAR), Singapore, and is currently working as a Member of Technical Staff and leading the Biomedical IC group and Analog & Mixed-Signal IC group in the Integrated Circuits and Systems Laboratory. Since he joined IME, he has led various projects developing a low-power 3-D accelerometer ASIC for high-end medical motion sensing applications, a readout ASIC for nanowire biosensor arrays detecting DNA/RNA and protein biomarkers for point-of-care diagnostics, an ultra-low-power sensor node SoC for continuous real-time wireless health monitoring, a wireless implantable sensor ASIC for medical devices, and MEMS interface & control SoCs for consumer electronics. His main research areas are low-power analog & mixed-signal circuits and systems interfacing with Bio and MEMS sensors, circuit design and multi-functional system integration with novel nano-devices, and wireless telemetry circuits and systems for biomedical applications. He is also a Program Manager of NeuroDevices Program under A*STAR Science and Engineering Research Council (SERC) and an Adjunct Assistant Professor in the Department of Electrical and Computer Engineering at National University of Singapore (NUS).

Prof. Je currently serves on the Technical Program Committee of the IEEE International Solid-State Circuits Conference (ISSCC).